Journal of Hazardous Materials 408 (2021) 124890

Contents lists available at ScienceDirect

Journal of Hazardous Materials

journal homepage: www.elsevier.com/locate/jhazmat

Research paper

Photocatalytic graphitic carbon nitride-chitosan composites for pathogenic biofilm control under visible light irradiation

Hongchen Shen [a], David P. Durkin [b], Ashlee Aiello [b], Tara Diba [c], John Lafleur [d], Jason M. Zara [c], Yun Shen [e,*], Danmeng Shuai [a,*,1]

[a] Department of Civil and Environmental Engineering, The George Washington University, Washington, DC, 20052 USA
[b] Department of Chemistry, United States Naval Academy, Annapolis, MD, 21402 US
[c] Department of Biomedical Engineering, The George Washington University, Washington, DC, 20052 USA
[d] Department of Emergency Medicine, George Washington University School of Medicine, Washington, DC, 20037 USA
[e] Department of Chemical and Environmental Engineering, University of California, Riverside, CA, 92521 USA

ARTICLE INFO

Editor: Dr. T Meiping

Keywords:
Biofilm
Graphitic carbon nitride
Chitosan
Visible-light-responsive Photocatalyst

ABSTRACT

Photocatalysis holds promise for inactivating environmental pathogens. Visible-light-responsive composites of carbon-doped graphitic carbon nitride and chitosan with high reactivity and processability were fabricated, and they can control pathogenic biofilms for environmental, food, biomedical, and building applications. The broad-spectrum biofilm inhibition and eradication of the photocatalytic composites against *Staphylococcus epidermidis*, *Pseudomonas aeruginosa* PAO1, and *Escherichia coli* O157: H7 under visible light irradiation were demonstrated. Extracellular polymeric substances in *Escherichia coli* O157: H7 biofilms were most resistant to photocatalytic oxidation, which led to reduced performance for biofilm removal. $^1O_2$ produced by the composites was believed to dominate biofilm inactivation. Moreover, the composites exhibited excellent performance for inhibiting biofilm development in urine, highlighting the promise for inactivating environmental biofilms developed from multiple bacterial species. Our study provides fundamental insights into the development of new photocatalytic composites, and elucidates the mechanism of how the photocatalyst reacts with a microbiological system.

1. Introduction

Environmental pathogens can persist in the environment and are ubiquitously found in the water, soil, air, food, and on contact surfaces (Yang et al., 2019; Ma et al., 2015; Yang et al., 2020). They can cause diseases with a measurable frequency after being introduced into human bodies, presenting serious health concerns and economic losses (Cangelosi et al., 2005). According to reports from the World Health Organization (WHO), 29% of the world population lacks access to safe drinking water, and every year more than 500,000 people die from the drinking water contaminated by rotavirus and *Escherichia coli* (*E. coli*) (World Health Organization, 2017). The U.S. Center for Disease Control and Prevention (CDC) estimated that more than 14,000 illnesses were caused by foodborne diseases in 2017, and that corresponding economic losses are approximately $7 billion annually (Centers for Disease Control and Prevention, 2019). SARS-CoV-2, the causative agent that leads to COVID-19 pandemic, is also environmentally persistent and can survive on different surfaces for several hours to days, which may lead to virus transmission via fomites (Van Doremalen et al., 2020). Environmental pathogens are most commonly associated with biofilms that reside on various surfaces, including but not limited to drinking water distribution systems, medical devices and equipment, food processers or packages, historic buildings, and sanitary wares (Cangelosi et al., 2005; Lu et al., 1999). These biofilms may contain bacteria, viruses, fungi, and parasites and cause many harmful issues such as drinking water contamination, nosocomial infections (e.g., catheter-associated urinary tract infections (CAUTIs)), food spoilage, and foodborne diseases (López-Guerra et al., 2019; Srey et al., 2013; Siqueira et al., 2011; Lacroix-Gueu et al., 2005). Specifically, biofilm-based CAUTIs are the leading cause of nosocomial infections (up to 40%) (Johnson et al., 2006).

Compared with environmental pathogens in a planktonic form, biofilms are much more persistent under harsh environmental conditions. One reason is that extracellular polymeric substances (EPS) in biofilms provide a favorable environment for microorganism survival

* Corresponding authors.
E-mail addresses: yun.shen@ucr.edu (Y. Shen), danmengshuai@gwu.edu (D. Shuai).
[1] Website: http://materwatersus.weebly.com/

https://doi.org/10.1016/j.jhazmat.2020.124890
Received 22 September 2020; Received in revised form 5 December 2020; Accepted 15 December 2020
Available online 18 December 2020

(Flemming and Wingender, 2010). Also, microorganisms within biofilms show a reduced metabolic activity and growth rate to slow down the uptake of antimicrobials (Davies, 2003). Specifically, biofilms on urinary catheter surfaces in vivo can tolerate antibiotics with concentrations up to three orders of magnitude higher than planktonic bacteria (Nickel et al., 1985). A number of methods have been proposed for controlling biofilms, including antibiotics delivery, metal ion inactivation (Ag^{+}, Cu^{2+}), quorum quenching, chemical oxidation (e.g., chlorine, peroxides, ozone), ultraviolet (UV) light irradiation, heating, detergent cleaning, and mechanical washing and scrubbing (Koo et al., 2017; Evans, 2003). In recent years, novel self-cleaning materials have attracted great attention in tackling the challenges of surface contamination by pathogenic biofilms (Huang et al., 2020). Nevertheless, most self-cleaning materials developed to date still have several major limitations. In particular, though antimicrobials can be incorporated into self-cleaning material matrices and their controlled release can inhibit biofilm development on surfaces, the antimicrobials are eventually depleted, and the self-cleaning feature is lost (Majeed et al., 2019). Other self-cleaning materials slow down biofilm formation by physically damaging bacteria (e.g., penetration of cell membranes through the sharp edge of 2D nanomaterials) or reducing bacterial adhesion (e.g., addition of hydrophilic functional groups to reduce bacterial adsorption). However, their performance in extended duration is questionable, because biofilms can still propagate with the aid of conditioning films (Farid et al., 2018). Moreover, some antimicrobials (e.g., antibiotics) selectively target a certain type of bacteria but not for others. Cooperation among different bacterial species in biofilms can further attenuate the effectiveness of antimicrobials (Becerril et al., 2020; Okuda et al., 2012). Finally, the emergence of antimicrobial resistance (e.g., antibiotic resistance) further challenges the safety and practical performance of some self-cleaning materials (Yuan et al., 2021). Therefore, there is a pressing need for developing effective, broad-spectrum, scalable, and robust strategies for controlling pathogenic biofilms in different environments.

Recently, our group has reported that a novel visible-light-responsive photocatalyst, carbon-doped graphitic carbon nitride (g-C_3N_4), holds promise for both inhibiting biofilm development and eradicating mature biofilms (Zheng et al., 2016; Shen et al., 2019). This photocatalyst can harvest photons with a wavelength shorter than 460 nm (experimentally determined bandgap is 2.72 eV, and conduction and valence band energy levels estimated by density functional theory simulations are −1.01/−0.67 and 1.57/2.28 eV, respectively). Hence the photocatalyst is reactive under the irradiation of fluorescent lamps and white light emitting diodes (LEDs), which is suitable for indoor environment applications and avoids complex installation, operation, and maintenance of UV lamps (Zheng et al., 2017; Liang et al., 2021). During photocatalysis, carbon-doped g-C_3N_4 converts oxygen gas continuously into reactive oxygen species (ROS, i.e., $O_2^{\cdot-}$, H_2O_2, $^1O_2$), and these inexhaustible ROS inactivate bacteria within biofilms by fast and effective reactions with biomacromolecules. No other chemicals are needed to assist photocatalytic oxidation, e.g., H_2O_2 (Liu et al., 2018). In addition, EPS, key building blocks in biofilms that support biofilm development and survival, were decomposed and removed after photocatalysis. Chemical oxidation in photocatalysis has been shown to break down the integral and cohesive structure of biofilms and facilitate complete biofilm removal, as opposed to slowing biofilm propagation (Shen et al., 2019). Furthermore, in contrast to antibiotics and many other antimicrobials, there is a lower likelihood for bacteria to develop resistance against photocatalysis because ROS react with biomacromolecules rapidly and non-selectively (Maisch, 2015). Therefore, photoreactive carbon-doped g-C_3N_4 can overcome the drawbacks of other anti-biofilm strategies, and it enables the development of emerging and innovative self-cleaning materials for pathogenic biofilm control.

Despite the advantages of applying carbon-doped g-C_3N_4 in biofilm control, one major limitation of this material is its poor processability for fabricating self-cleaning surfaces. Synthesis of carbon-doped g-C_3N_4 using thermal polycondensation always results in a powder form, and it is challenging to use this powdered material as a coating or in the development of continuous and robust self-cleaning materials. To address this concern, chitosan was selected as a polymer matrix to hold the photocatalyst (Zheng et al., 2020). Chitosan is a partial deacetylation derivative of chitin which constitutes the exoskeleton of crustaceans such as shrimp. Chitosan has desirable characteristics that enable broad engineering applications (e.g., biodegradability, biocompatibility, economic feasibility, scalability), and incorporating the photocatalyst powder of carbon-doped g-C_3N_4 into chitosan confers upon the composites improved processability for developing self-cleaning surfaces (Lin et al., 2020; Midya et al., 2019). Depending on the applications, these composites can be easily tailored to different shapes and dimensions (e.g., thin films for food packaging, internal coatings for urinary catheters).

In this study, we synthesized a photocatalytic and self-cleaning composite by incorporating carbon-doped g-C_3N_4 into a chitosan matrix for inactivating and eradicating biofilms from *Staphylococcus epidermidis*, *Pseudomonas aeruginosa* PAO1, *Escherichia coli* O157: H7 (a foodborne pathogen), and from mixture of bacterial species in urine of urinary tract infections (UTI) patients. To understand the physical, chemical, thermal, and morphological properties of this composite, scanning electron microscopy (SEM), attenuated total reflectance-Fourier transform infrared spectroscopy (ATR-FTIR), thermal gravimetric (TG) analysis, and Brunauer-Emmett-Teller (BET) surface area analysis were conducted. To determine the antimicrobial performance of the composite under visible light irradiation, the viability, composition, morphology, and coverage of biofilms developed on the self-cleaning composite were comprehensively examined by confocal laser scanning microscopy (CLSM), optical coherence tomography (OCT), and SEM. Moreover, to elucidate the mechanisms of how this composite controlled biofilms, ROS quenching experiments were conducted.

2. Experimental

2.1. Synthesis of carbon-doped g-C_3N_4 powder and fabrication of its chitosan composites (i.e., photocatalyst-chitosan composites)

Carbon-doped g-C_3N_4 was synthesized as described in our previous study (Zheng et al., 2016). For developing its chitosan composite, 1 g of the photocatalytic powder and 1 g of chitosan were amended into 40 mL of acetic acid solution (2.5%, v/v) and dispersed by probe ultrasonication (300 W) for 1 h. Next, the mixture was magnetically stirred until a uniform emulsion was obtained. 0.2 mL of crosslinker, i.e., epichlorohydrin, was added into the emulsion and the mixture was magnetically stirred for additional 4 h at the room temperature. Crosslinking significantly reduces the solubility of chitosan in water, and thus enhances the practicality of this composite for engineering applications especially in contact with water. After crosslinking, 1 mL of emulsion was placed in a plastic mold with a dimension of 2 cm × 2 cm and dried at the room temperature overnight. The obtained composite was peeled off from the mold and rinsed by 1 M NaOH solution for 2 h to neutralize residual acetic acid. Finally, the composite was washed to a neutral pH with ultrapure water for several times. The developed composites of carbon-doped g-C_3N_4 and chitosan were utilized for all antimicrobial experiments. Chitosan-only films were also developed with the same procedure as control samples, without introducing the carbon-doped g-C_3N_4 powder.

2.2. Material characterization of photocatalyst-chitosan composites and chitosan-only films

The photocatalyst-chitosan composites and chitosan-only films were characterized by ATR-FTIR, BET surface area analysis, SEM, and TG analysis. Details are included in our previous study (Zheng et al., 2020).

2.3. Biofilm inhibition and eradication on the photocatalyst-chitosan composites and composite stability

To demonstrate the broad-spectrum antimicrobial activity of the photocatalyst-chitosan composite, different microorganisms including *Staphylococcus epidermidis* (*S. epidermidis*, Gram-positive, ATCC 35984), *Pseudomonas aeruginosa* PAO1 (*P. aeruginosa* PAO1, Gram-negative, ATCC 47085), and one notorious foodborne pathogen *Escherichia coli* O157: H7 (*E. coli* O157: H7, Gram-negative, ATCC 43894) were selected to develop single-species biofilms on the surface of the photocatalyst-chitosan composite.

Biofilm development from single bacterial species and biofilm inhibition and eradication followed the procedure described in our previous study with minor revisions (Shen et al., 2019). Specifically, for biofilm development, *S. epidermidis* and *E. coli* O157: H7 were cultured on the photocatalyst-chitosan composite surfaces in 6 mL of 10-fold diluted tryptic soy broth (TSB) for 3 days in the dark, while *P. aeruginosa* PAO1 was cultured on the composite surface in 6 mL of 50-fold diluted TSB for 7 days in the dark. For biofilm inhibition, the photocatalyst-chitosan composites were placed under continuous irradiation of a white LED lamp (7 W) with the same duration and medium conditions as described in biofilm development for each bacterial strain. The TSB media for biofilm development and inhibition experiments were replenished every 24 h. For biofilm eradication, mature *S. epidermidis* and *P. aeruginosa* PAO1 biofilms on the composite surfaces were exposed to white LED light for 1 day in phosphate buffered saline (PBS). However, more challenging conditions were adopted for mature *E. coli* O157:H7 biofilms, including using a blue LED lamp or a shorter distance between the lamp and the PBS solution to increase the light intensity and extending light exposure duration. The corresponding photon flux and the optical power density could be utilized in photocatalysis were summarized in the Table S1.

To investigate the stability of the composite material during photocatalysis, the composites were challenged by three continuous cycles of photocatalytic inhibition experiments against *S. epidermidis* biofilms. For each cycle, the composites were first submerged in bacteria-PBS solution (OD_{600} =0.5) in the dark for 24 h to allow bacterial adsorption. Next, the bacteria-PBS solution was replaced with 6 mL of 10-fold diluted TSB. One group of composites was exposed to continuous white LED light irradiation (7 W) for 3 days. Another group of composites was kept in the dark for 3 days. Other experimental conditions like temperature (37 °C), mixing rate (80 rpm), and daily replenishment of 10-fold diluted TSB were the same for both groups. After one cycle of experiment, some composites were sacrificed for biofilm viability assessment, while the other composites were washed with sterilized DI water thoroughly to remove biofilms or residual microorganisms for biofilm regrowth in the next cycle.

2.4. Biofilm inhibition on the photocatalyst-chitosan composites in patient urine

To further explore the potential of applying the antimicrobial photocatalyst-chitosan composites in medical devices (e.g., developing antimicrobial urinary catheters) and sanitary wares, the inhibition of multi-species biofilms developed from UTI patient urine was evaluated. Patients were 18 years or older, and arrived at the Emergency Department of The George Washington University Hospital (Washington, DC) with one or more urinary symptom(s) (e.g., burning, increased frequency, flank pain, nausea/emesis, and chills) and urine white blood cell counts more than 10 per high power field. Patients were excluded from the study if they did not understand consent (i.e., under the influence of drugs, alcohol, or cognitively impaired) or had been treated with antibiotics before obtaining the urine samples. Patients who agreed to participate in the study reviewed their urinary symptom(s) with study personnel, gave permission for the research team to extract relevant patient and treatment information, and signed written informed consent. Study personnel documented patient age, gender, vital signs, urinary symptoms, and selected laboratory test results.

The photocatalyst-chitosan composites were placed in sterile six-well plates and submerged by 6 mL of infected urine. For the inhibition tests, the system was placed under continuous blue LED light (7 W) irradiation for 6 days, and the distance between the blue LED lamp and the surface of urine was maintained at 6 cm. Compared with the white LED light used in Section 2.3, blue LED light used in the urine experiment showed a higher intensity that can be utilized by carbon-doped g-C_3N_4 (the spectral irradiance of both light sources were recorded in Fig. S1). For the control study, a composite with urine was kept in the dark for 6 days. Other conditions like temperature (37 °C) and mixing rate (80 rpm) were the same for both studies.

2.5. Optical coherence tomography (OCT) for characterizing biofilm thickness and coverage

In this study, different biofilms on the surface of the photocatalyst-chitosan composites were directly visualized by a Ganymede II (Thorlabs Inc.) Spectral Domain OCT system. OCT images were processed using the software ImageJ (https://imagej.nih.gov/ij/). Biofilms were first outlined manually, and the corresponding average thickness and coverage were calculated with the same method described in our previous study (Shen et al., 2019).

2.6. Confocal laser scanning microscopy (CLSM) for characterizing bacterial viability and extracellular polymeric substances (EPS) within biofilms

The Filmtracer™ LIVE/DEAD® Biofilm Viability Kit and the Invitrogen™ Molecular Probes™ Wheat Germ Agglutinin (WGA, Alexa Fluor™ 488 Conjugate) were used to evaluate bacterial viability within different biofilms and to characterize EPS abundance and distribution within *S. epidermidis* biofilms, respectively. Sample preparation, CLSM operation, and the calculation of the ratio of live to dead cells in the biofilms were described in our previous study (Shen et al., 2019).

2.7. Scanning electron microscopy (SEM) for characterizing biofilm morphology

The photocatalyst-chitosan composites with biofilms were gently rinsed by PBS once to remove loosely bounded biomass, and the samples were immediately placed into the −20 ℃ fridge overnight. Next, the frozen samples were freeze dried. Before SEM imaging, the samples were sputter-coated with iridium to prevent sample charging. The biofilm samples were examined using a FEI Teneo LV FEG SEM. The freeze-drying method was used for biofilm characterization and it can retain as much as biomass for analysis. This method is advantageous compared with the fixation method with glutaraldehyde and paraformaldehyde because it avoids multiple steps of biofilm rinsing that leads to significant biomass loss.

2.8. Identification and quantification of reactive oxygen species (ROS) in photocatalysis for biofilm control

Radical probes that specifically react with certain ROS were utilized to identify and quantify ROS generated during photocatalysis. Specifically, *para*-chlorobenzoic acid (*p*-CBA), furfuryl alcohol (FFA), and 2, 3-bis (2-methoxy-4-nitro-5-sulfophenyl)− 2*H*-tetrazolium-5-carboxanilide (XTT) were used to detect ·OH, $^1O_2$, and $O_2^{\cdot-}$, respectively. In addition, the accumulated concentration of H_2O_2 was quantified by a colorimetric method with *N*,*N*-diethyl-*p*-phenylenediamine sulfate salt (DPD). Details can be found in our previous study (Shen et al., 2019; Zheng et al., 2019).

To identify the most important ROS for inactivating biofilms, ROS quenching experiments were also conducted. The photocatalyst-

chitosan composite coated glass slide (Fig. S2) was prepared, loaded with planktonic bacteria of *S. epidermidis*, and subjected to photocatalysis with ROS scavengers. Bacterial viability was determined by CLSM and compared in the presence or absence of the ROS scavengers to elucidate the critical role of a certain ROS. Briefly, the glass slide was first dipped into the emulsion prepared from carbon-doped g-C_3N_4 and chitosan (after crosslinking), as described in the Section 2.1, for 20 s, and drawn vertically. After being dried at the room temperature overnight, the glass slide was soaked in 1 M NaOH for 1 h and washed by ultrapure water to a neutral pH, and it was ready to use. *S. epidermidis* PBS suspensions without any scavenger, with 10 mM FFA ($^1O_2$ scavenger), or with 1 mM 4-hydroxy-2,2,6,6-tetramethylpiperidine 1-oxyl (4-hydroxy-TEMPO, $O_2^{\cdot-}$ scavenger) but with the same bacterial concentration were prepared, and 50 μL of the suspension was aspirated and dropped onto the composite coated glass slides. The suspension droplets on the glass slides were then placed in the dark or under the white LED light irradiation for 1 h (the distance between the surface of the slide and the 7 W white LED lamp was maintained at 15 cm). All the samples were finally stained by the Filmtracer™ LIVE/DEAD® Biofilm Viability Kit as instructed in the manual and characterized by a Carl Zeiss 710 Spectral Confocal Microscope equipped with a 63 × oil immersed objective to understand bacterial viability with or without the presence of ROS scavengers.

3. Results and discussion

3.1. Material characterizations of the photocatalyst-chitosan composite

The synthesis of carbon-doped g-C_3N_4 powder and the characterization of its physical, morphological, chemical, and optical properties have been reported previously (Zheng et al., 2016). Carbon-doped g-C_3N_4/chitosan composite films were developed for the first time, and they were characterized and compared with chitosan-only films. The successful incorporation of photocatalyst into the chitosan matrix was demonstrated by SEM. Compared with photocatalyst-chitosan composites, chitosan-only films possessed a smoother surface (Fig. 1a). Photocatalyst particles were uniformly distributed on the composite surface, which is crucial for effective photocatalysis and biofilm inhibition and eradication (Fig. 1b). The surface area of photocatalyst-chitosan composites (0.283 ± 0.005 $m^2\ g^{-1}$) was higher than that of chitosan-only films (0.045 ± 0.001 $m^2\ g^{-1}$), indicating increased surface roughness (Fig. 1c). These small surface areas showed neither material was porous, which is in contrast to the g-C_3N_4/chitosan hydrogel beads fabricated in our previous study (Zheng et al., 2020). The non-porous structure of the materials enables them as promising coating materials and prevents potential liquid or gas penetration in engineering and biomedical applications. ATR-FTIR did not show significant differences between chitosan-only films and photocatalyst-chitosan composites (Fig. 1d): both spectra showed features expected for chitosan, i.e., 3300–3500 cm^{-1} (O–H and N–H stretches), 1030 cm^{-1} (C–O stretch), and a series of peaks within 1300–1650 cm^{-1} (C–N heterocycle stretching vibrations) (Kumirska et al., 2010). Since carbon-doped g-C_3N_4 has similar functional groups (e.g., N–H, -NH_2, or C–N), the influence of photocatalyst incorporation into the chitosan matrix on the FTIR spectra might be overlapped and difficult to discern; however, the data indicated the g-C_3N_4 was not chemically bonded to the support. TG analysis showed that the maximum temperature for thermal decomposition of chitosan-only films during pyrolysis was 286–289 °C and for g-C_3N_4 was ca. 660–680 °C (Fig. 1e). The derivative thermograms (DTG) more clearly showed these regions of interest, and both peaks were present as well in the photocatalyst-chitosan composites (Fig. 1f). These data support the conclusion from SEM and ATR-FTIR that the g-C_3N_4 was physically incorporated but not chemically bonded to the chitosan matrix. Due to the high processability of the liquid precursor, the photocatalyst-chitosan composites could be tailored into different shapes by using molds (Fig. 1g). The mechanical performance of the composites was enhanced by crosslinking and the composites were flexible and could be easily bent especially when they were wet (Fig. 1h).

3.2. Broad-spectrum biofilm inhibition on photocatalyst-chitosan composites

In contrast to lab-grown biofilms, biofilms developed in natural environments, engineering systems, and biomedical settings, always contain multiple bacterial species, and developing a broad-spectrum antimicrobial material that can effectively inactivate (almost) all pathogens is a pressing need for practical applications (Schwering et al., 2013). In general, many antimicrobials (e.g., antibiotics) only selectively inhibit the growth of a certain kind of pathogenic bacteria, and a single one cannot simultaneously inactivate all pathogens effectively. Carbon-doped g-C_3N_4 produces ROS in photocatalysis, which is expected to effectively and rapidly inactivate a broad-spectrum of pathogenic bacteria because of non-selective reactions between ROS and biomolecules in different bacterial species. In this study, three representative bacteria, *S. epidermidis*, *P. aeruginosa* PAO1, and *E. coli* O157: H7 were selected to demonstrate the broad-spectrum antimicrobial potential of the photocatalyst-chitosan composites under visible light irradiation. *S. epidermidis* and *P. aeruginosa* PAO1, a Gram-positive and Gram-negative bacterium, respectively, are responsible for a host of nosocomial infections (Preston et al., 1997; Vuong and Otto, 2002). There are huge differences in structures between Gram-positive and Gram-negative bacteria. Thick, multiple layers of peptidoglycan envelope the Gram-positive bacterial plasma membrane, while a complicated sandwich-like structure, including an outer membrane, a single intermediate peptidoglycan layer, and an inner membrane, is shown in the Gram-negative bacteria (Rogers, 2010). Due to their different structural characteristics, Gram-negative and Gram-positive bacteria may have different sensitivities to any given antimicrobial agent. *E. coli* O157: H7, a notorious foodborne pathogen, produces potent bacterial toxins, known as Shiga toxin, and has become a major challenge for food safety (Melton-Celsa, 2015). Biofilms formed by *S. epidermidis*, *P. aeruginosa* PAO1, and *E. coli* O157: H7 are commonly found on the surfaces of implantable medical devices or food processers and contact surfaces. As a consequence, efficient inhibition and eradication of these biofilms is a primary concern in preventing foodborne disease outbreaks or nosocomial infections.

Under the continuous irradiation of white LED light, the photocatalyst-chitosan composites exhibited excellent biofilm inhibition performance against *S. epidermidis*, *P. aeruginosa* PAO1, and *E. coli* O157: H7. After 3 days (for *S. epidermidis* and *E. coli* O157: H7) or 7 days (for *P. aeruginosa* PAO1) culturing in the dark, biofilms formed by all bacterial strains were found to be flourishing on the composite surfaces and most bacteria were alive as observed by CLSM (Fig. 2a, c, and e, CLSM). Limited antimicrobial effect in the absence of light indicates that the composites are biocompatible, making them promising candidates for food or biomedical applications (e.g., food packages, food contact surface coatings, and urinary catheter coatings). Only a few isolated, live bacteria were found on composite surfaces under light irradiation (Fig. 2b, d, and f, CLSM). Bacteria were speculated to settle down to the composite surfaces from the nutritious media due to gravity, but they were continuously inactivated by ROS and/or holes generated in photocatalysis and removed by the shear forces from mixing. No biofilms propagated on the photocatalyst-chitosan composites under visible light irradiation, indicating the visible light enabled the self-cleaning nature of the composite. On the basis of OCT analyses, the average thickness of biofilms formed by *S. epidermidis*, *P. aeruginosa* PAO1, and *E. coli* O157: H7 on the composite surfaces in the dark was 97.4 ± 68.3, 81.0 ± 115.1, and 33.8 ± 12.7 μm, respectively. The coverage of biofilms of *S. epidermidis*, *P. aeruginosa* PAO1, and *E. coli* O157: H7 was 96%, 39%, and 100%, respectively (Fig. 2a, c, and e, OCT). However, biofilms could

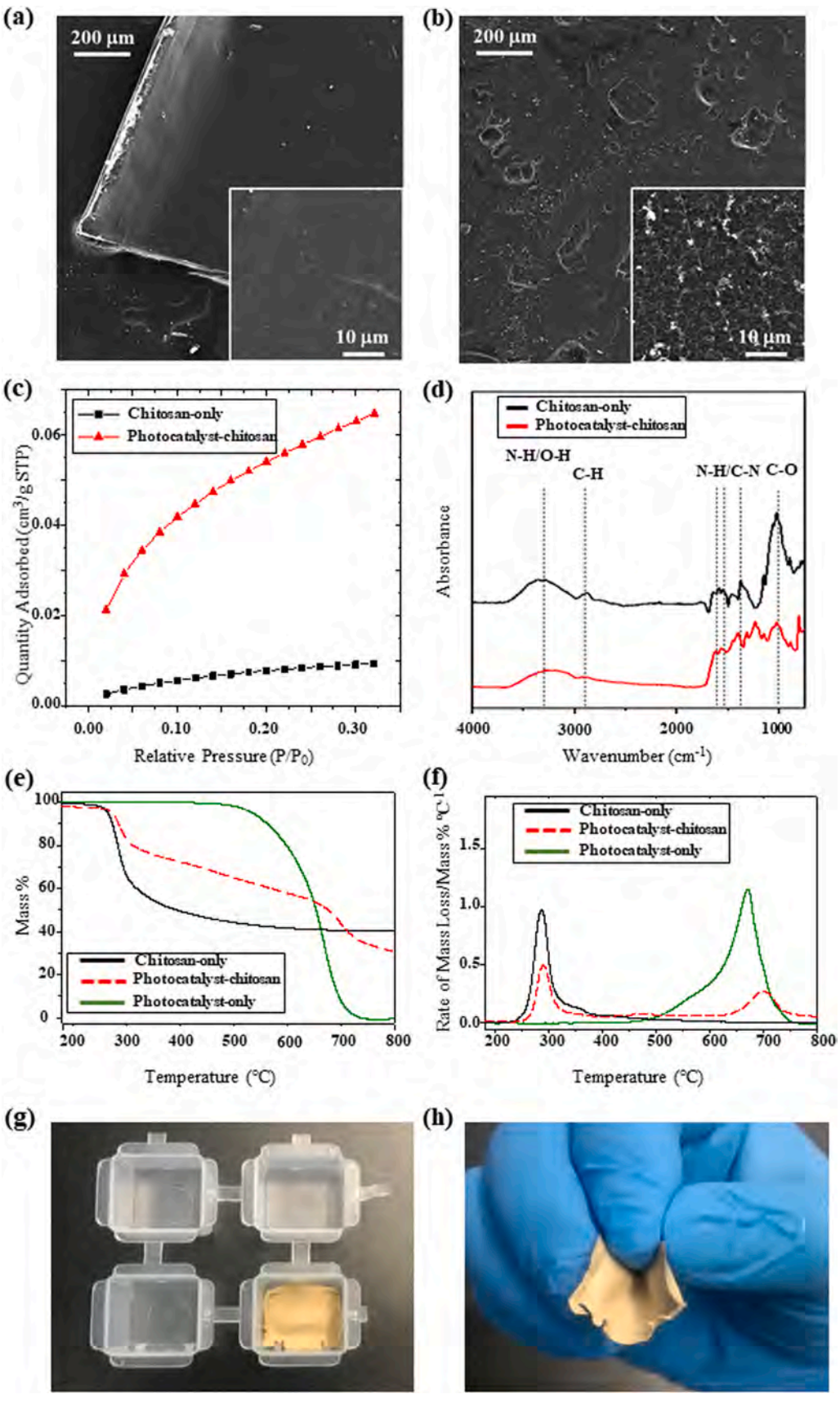

Fig. 1. Material characterizations for both the chitosan-only films and the photocatalyst-chitosan composites. SEM images of (a) the chitosan-only film and (b) the photocatalyst-chitosan composite, (c) N_2 adsorption/desorption isotherms of the chitosan-only film and the photocatalyst-chitosan composite, (d) ATR-FTIR spectra of the chitosan-only film and the photocatalyst-chitosan composite, (e) TG and (f) DTG analyses of the chitosan-only film and the photocatalyst-chitosan composite, (g) one photocatalyst-chitosan composite casted in a square mold, and (h) one flexible, wet photocatalyst-chitosan composite. (For interpretation of the references to colour in this figure legend, the reader is referred to the web version of this article.)

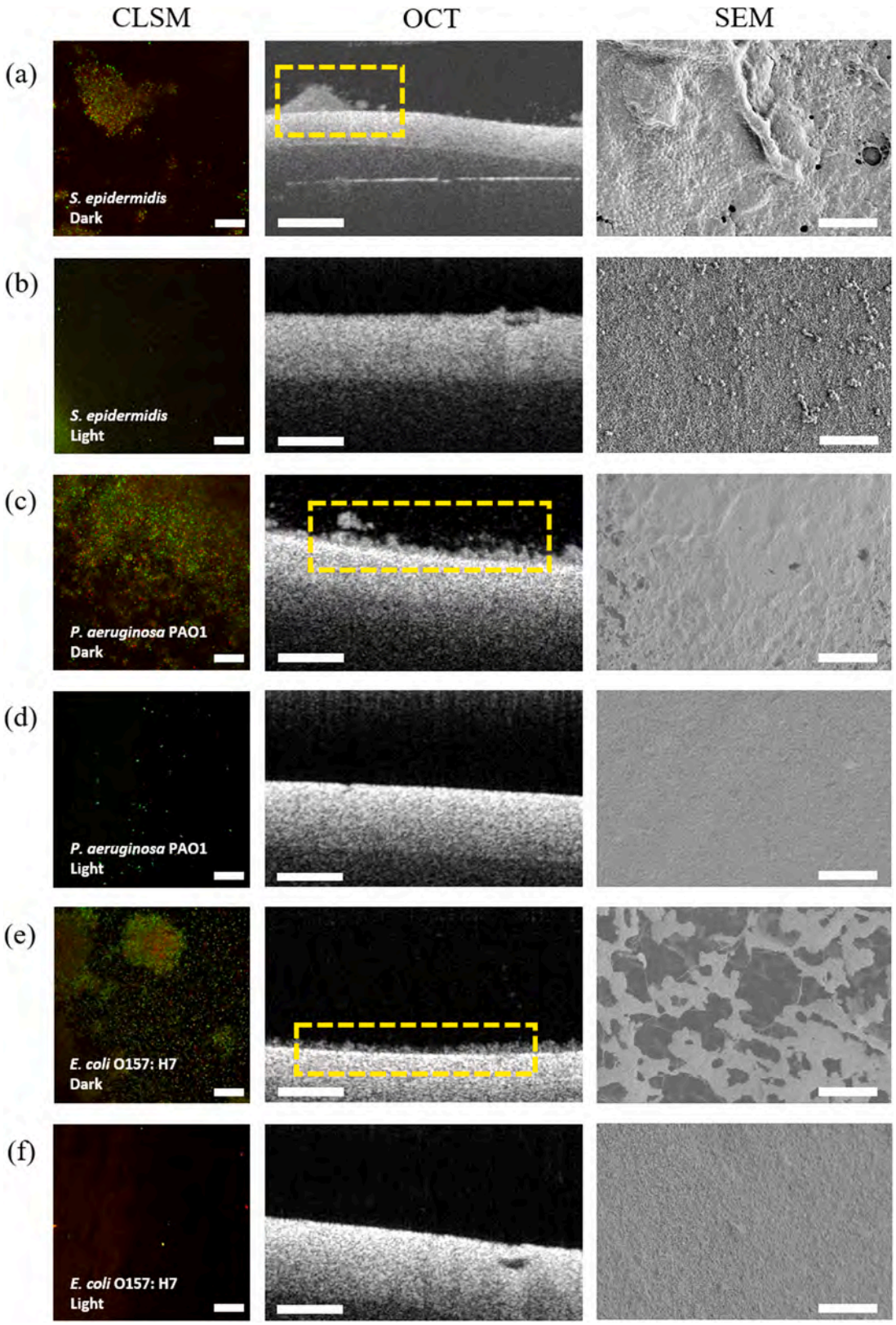

Fig. 2. Broad-spectrum biofilm inhibition of the photocatalyst-chitosan composites under visible light irradiation. Two dimensional-CLSM (2D-CLSM) images, OCT images, and SEM images of (a) *S. epidermidis*, (c) *P. aeruginosa* PAO1, and (e) *E. coli* O157: H7 biofilms cultured on the composite surfaces in the dark, respectively; 2D-CLSM images, OCT images, and SEM images of (b) *S. epidermidis*, (d) *P. aeruginosa* PAO1, and (f) *E. coli* O157: H7 biofilms cultured on the composite surfaces under continuous white LED light irradiation (7 W). Scale bars in 2D-CLSM, OCT, and SEM images are 20, 200, and 10 μm, respectively. Biofilms in OCT images are highlighted by yellow dashed rectangles. The distance between the light source and the solution that submerged the photocatalyst-chitosan composites was maintained at 15 cm. (For interpretation of the references to colour in this figure legend, the reader is referred to the web version of this article.)

rarely be observed on the composite surfaces under light irradiation through OCT, indicating broad-spectrum biofilm inhibition under light irradiation (Fig. 2b, d, and f, OCT). In addition, biofilm aggregates in which bacteria were encapsulated by abundant EPS were observed in the dark samples (Fig. 2a, c, and e, SEM), while only isolated bacteria and/or a clean surface were found when the composites were exposed to light irradiation (Fig. 2b, d, and f, SEM), which is consistent with results from CLSM and OCT.

In contrast to dense and healthy biofilms on the composite surfaces developed in the dark (Fig. 3d, e, and f), no *S. epidermidis* biofilms were observed under visible light irradiation for three continuous cycles (Fig. 3a, b, and c), which demonstrated the composites could be used for long-term antimicrobial applications. In addition, the photocatalyst-chitosan composites remained robust and integrated after three cycles of experiments (Fig. S3), highlighting the material stability.

3.3. Broad-spectrum biofilm eradication from photocatalyst-chitosan composites

For many practical applications, photoreactive self-cleaning composites may not always be exposed to light, and biofilms could inevitably form and propagate under that circumstance. In addition, compared with planktonic bacteria, biofilms are much more resistant to conventional disinfection or removal methods once they are formed on a surface (Davies, 2003). Eradicating mature biofilms from the surface is more challenging compared with inhibiting new biofilm development, because EPS in biofilms protect bacteria from inactivation or removal under stress. Therefore, besides biofilm inhibition, we also systematically evaluated the eradication of mature biofilms from the photocatalyst-chitosan composites under visible light irradiation to demonstrate the effectiveness of self-cleaning on mature biofilms.

In biofilm eradication experiments, the photocatalyst-chitosan composites showed promising eradication performance against biofilms formed by *S. epidermidis* and *P. aeruginosa* PAO1 under white LED light irradiation. After one day of light exposure, while the majority of mature *S. epidermidis* biofilms was removed from the composite surfaces, only a thin layer of isolated inactivated bacteria from the *P. aeruginosa* PAO1 biofilms was left on the composite surfaces (Fig. 4a and b, CLSM). OCT and SEM further confirmed the complete eradication of mature biofilms formed by both bacterial strains from the composite surfaces (Fig. 4a and b, OCT and SEM). For *E. coli* O157: H7, however, one day of white LED light exposure was not sufficient to inactivate and eradicate mature biofilms. There were still large aggregates of bacteria left on the composite surfaces though the ratio of live to dead cells in the biofilms decreased from 21.5 ± 2.8–0.5 ± 0.1 after one day of light treatment (Fig. 2e and Fig. 4c, CLSM). The average thickness of biofilms after light treatment was 34.8 ± 15.0 μm, which was comparable to the average thickness of biofilms cultured in the dark on the composite surfaces (33.8 ± 12.7 μm, Fig. 2e and Fig. 4c, OCT). In addition, SEM images clearly showed abundant residual EPS left on the composite surface after one day of white LED light exposure, indicating EPS within *E. coli* O157: H7 biofilms are much more resistant to photocatalysis (Fig. 4c, SEM). Extending the duration of white LED light exposure to 3 days still did not remove biofilms apparently: biofilms kept an average thickness of 35.4 ± 13.1 μm (Fig. 5d and Fig. S4). To promote biofilm eradication by increasing the oxidative stress, a blue LED lamp (flux of 1.38×10^3 μmol m^{-2} s^{-1} for photons with a shorter wavelength than 460 nm) instead of the white LED lamp (flux of 3.46×10^2 μmol m^{-2} s^{-1} for photons with a shorter wavelength than 460 nm) was used to increase available photons that could be utilized by photocatalytic carbon-doped g-C_3N_4 (Table S1). After 3 days of blue light exposure, OCT indicated that only a small portion of *E. coli* O157: H7 biofilms was left on the composite surfaces (Fig. 5a). In addition to OCT, CLSM provided more insights into the viability of biofilms: almost all bacteria within the *E. coli* O157: H7 biofilms were inactivated under blue LED light exposure for 3 days (Fig. 5b and c), whereas the bacteria were partially inactivated under white LED light exposure for the same duration (the ratio of live to dead cells was 0.6 ± 0.4, Fig. 5e and f). Control experiments were also performed, and they demonstrated that PBS without nutrients or blue LED light exposure alone did not inactivate bacteria within biofilms up to 7 or 3 days, respectively (Fig. S5). Increased light utilization and corresponding photoreactivity of the self-cleaning composites was able to eradicate tough biofilms developed from *E. coli* O157: H7 successfully, which suggests biofilm eradication is a kinetically controlled process. It is well-known that dispersion occurs when biofilms become mature, in which some bacteria leave the biofilms and find another place to colonize. Our study has demonstrated that the self-cleaning composites not only eradicate mature biofilms but also potentially inactivate dispersed bacteria to prevent their propagation by photocatalysis. Different efficiencies for mature biofilm removal developed from diverse

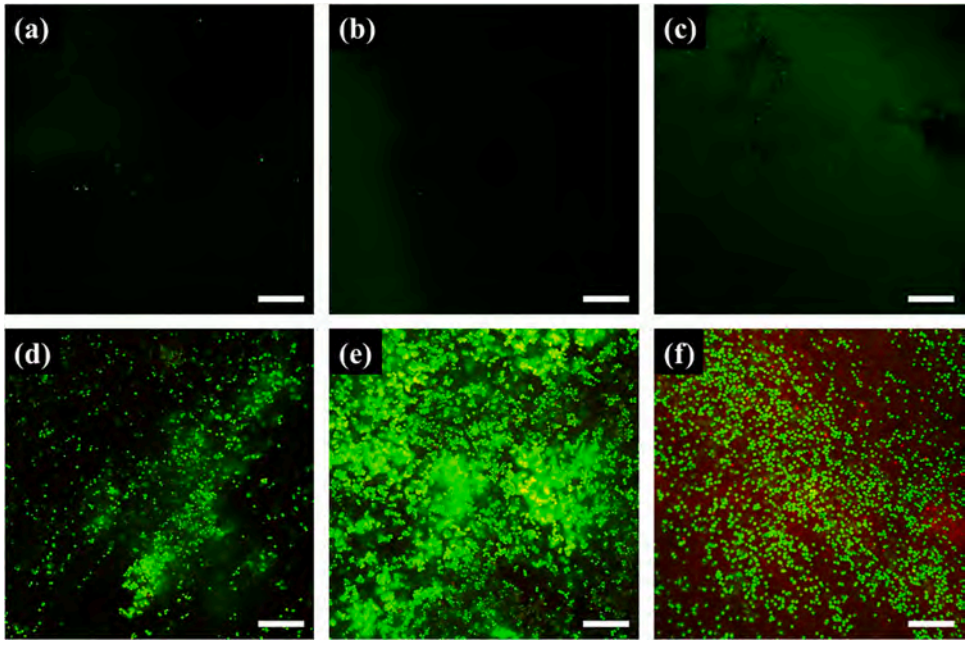

Fig. 3. Three continuous cycles of photocatalytic inhibition experiments against *S. epidermidis* biofilms. (a) First, (b) second, and (c) third cycle of *S. epidermidis* biofilms cultured on the photocatalyst-chitosan composite surfaces under continuous white LED light irradiation (7 W); and (d) first, (e) second, and (f) third cycle of *S. epidermidis* biofilms cultured on the composite surfaces in the dark. Scale bars are 20 μm. The distance between the light source and the solution that submerged the photocatalyst-chitosan composites was maintained at 15 cm. (For interpretation of the references to colour in this figure legend, the reader is referred to the web version of this article.)

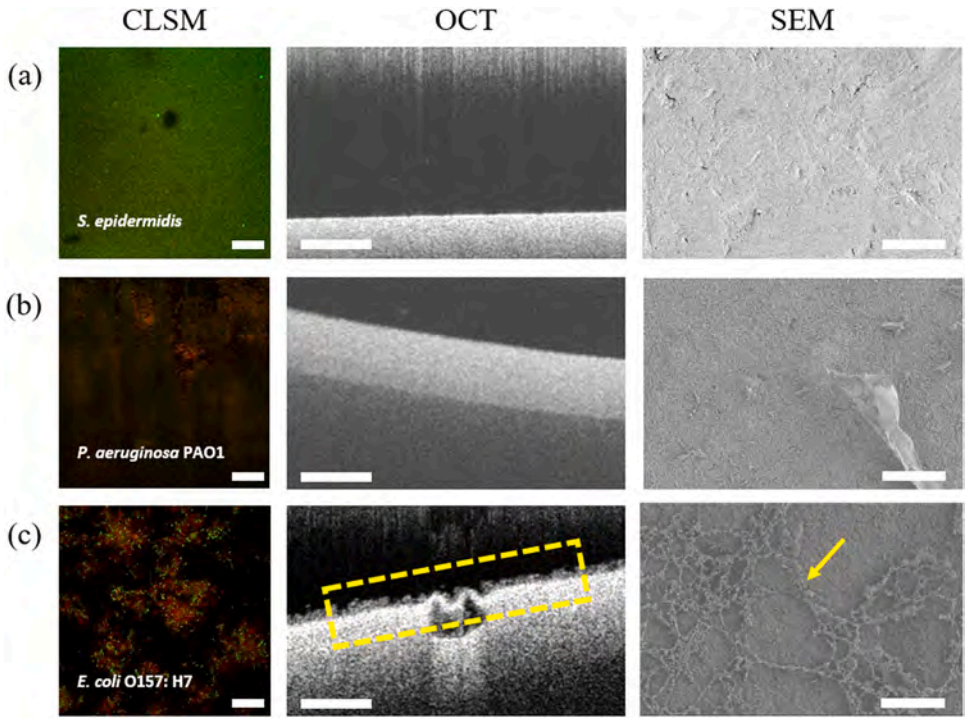

Fig. 4. Broad-spectrum biofilm eradication from the photocatalyst-chitosan composites under visible light irradiation. 2D-CLSM images, OCT images, and SEM images of (a) *S. epidermidis*, (b) *P. aeruginosa* PAO1, and (c) *E. coli* O157: H7 biofilms eradication from the composite surfaces under white LED light irradiation (7 W). Scale bars in 2D-CLSM, OCT, and SEM images are 20, 200, and 10 μm, respectively. Residual biofilms in OCT and SEM images are highlighted by yellow dashed rectangles and yellow arrows, respectively. The distance between the light source and the solution that submerged the photocatalyst-chitosan composites was maintained at 15 cm. (For interpretation of the references to colour in this figure legend, the reader is referred to the web version of this article.)

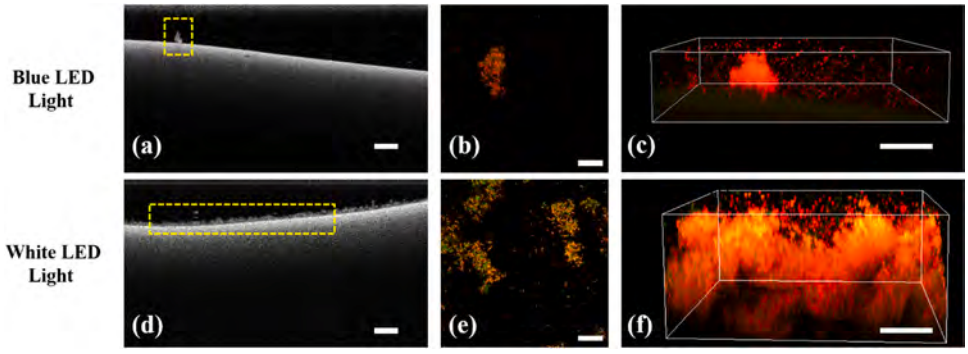

Fig. 5. Effect of enhanced light utilization on biofilm eradication from the photocatalyst-chitosan composites. (a) OCT image, (b) 2D-CLSM image, (c) three dimensional (3D)-CLSM image of mature *E. coli* O157: H7 biofilms on the composite surface after 3 days of blue LED light irradiation (7 W); (d) OCT image, (e) 2D-CLSM image, (f) 3D-CLSM image of mature *E. coli* O157: H7 biofilms on the composite surface after 3 days of white LED light irradiation (7 W). Scale bars in OCT, 2D-CLSM, and 3D-CLSM images are 250, 20, and 30 μm, respectively. Residual biofilms in OCT images are highlighted by yellow dashed rectangles. The distance between the light sources and the solution that submerged the photocatalyst-chitosan composites was maintained at 5 cm. (For interpretation of the references to colour in this figure legend, the reader is referred to the web version of this article.)

bacterial strains could be attributed to the distinct responses of EPS in biofilm matrices to photocatalysis, which will be elucidated in the next section..

3.4. Response of extracellular polymeric substances (EPS) to photocatalysis

EPS, which are mainly comprised of polysaccharides, proteins, lipids, and eDNA, perform multiple important functions, e.g., promoting biofilm adhesion to surfaces, bacterial cohesion, and biofilm survival and development (Flemming et al., 2007). EPS have been frequently reported to act as a protective barrier which prevents bacteria within biofilms from attack by antibiotics, oxidants, or other antimicrobials (Gao et al., 2015). Moreover, EPS are important for maintaining the 3D structure of the biofilms. Destructing EPS matrices makes bacteria within biofilms more vulnerable to antimicrobials and promotes biofilm removal. In our study, we characterized EPS of biofilms developed from *S. epidermidis*, *P. aeruginosa* PAO1, and *E. coli* O157: H7 before and after photocatalysis and identified the important role of EPS in biofilm eradication.

Before photocatalysis, bacteria within mature biofilms formed by all three bacterial strains were embedded in abundant EPS (Fig. 6a-c). Freeze drying was used to treat biofilm samples prior to SEM characterizations, instead of the fixation method used in the previous study (including multiple steps of fixation, rinsing, and ethanol dehydration), because freeze drying best preserves the 3D structure of mature biofilms (Fig. S6) (Shen et al., 2019). It is speculated that the shear forces generated by mild mixing during fixation, rinsing, and ethanol dehydration were responsible for the biofilm removal due to weak adhesion between biofilms and the composites with hydrogel nature. However, freeze drying inevitably shrunk or deformed bacterial cells based on SEM characterizations. After photocatalysis, while most EPS in *S. epidermidis* and *P. aeruginosa* PAO1 biofilms were removed and occasionally isolated bacteria were left on composite surfaces (Fig. 6d and

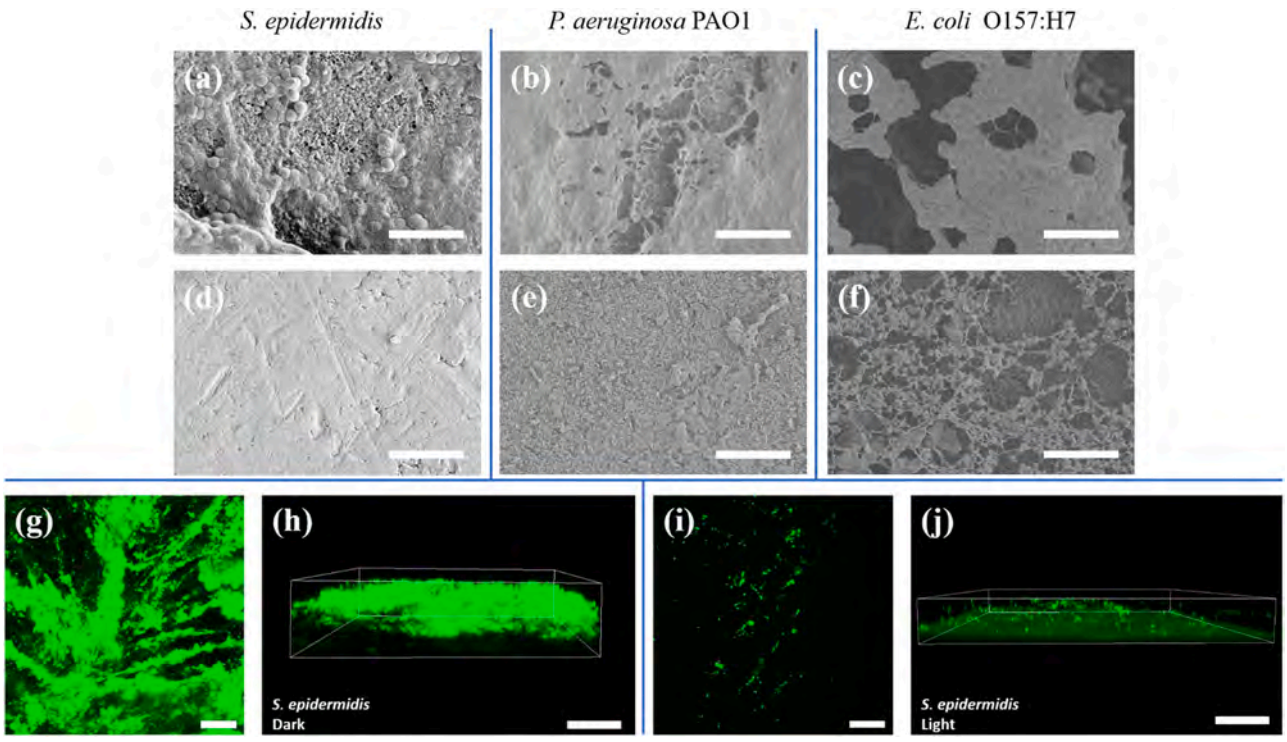

Fig. 6. Response of EPS in different biofilms to photocatalysis. SEM images of biofilms formed from *S. epidermidis*, *P. aeruginosa* PAO1, and *E. coli* O157: H7 on the photocatalyst-chitosan composite surfaces (a-c) before and (d-f) after one day of white LED light irradiation (7 W); CLSM images of *S. epidermidis* biofilms stained by the fluorescent-labeled WGA (g, h) before and (i, j) after one day of white LED light irradiation (7 W). Scale bars in SEM, 2D-CLSM, and 3D-CLSM images are 5, 20, and 30 μm, respectively. The distance between the light source and the solution that submerged the photocatalyst-chitosan composites was maintained at 15 cm.

e), the amount of EPS only slightly decreased in *E. coli* O157: H7 biofilms (Fig. 6f). Filamentous EPS left on the composite surfaces could be caused by the collapse of EPS matrices in dehydration (Dohnalkova et al., 2011). The results indicate that EPS in *S. epidermidis* and *P. aeruginosa* PAO1 biofilms were oxidized, decomposed, or removed by ROS generated during photocatalysis whereas EPS within *E. coli* O157: H7 biofilms were relatively more resistant to ROS. The EPS decomposition and removal of *S. epidermidis* biofilms during photocatalysis were also demonstrated by the fluorescent detection of polysaccharide intercellular adhesin (PIA) that is a major component in the EPS matrix of the *S. epidermidis* biofilms. For mature *S. epidermidis* biofilms formed on the composite surfaces in the dark, CLSM characterizations showed large aggregates of PIA within biofilms (Fig. 6g and h). For biofilms after photocatalysis, only small clusters of PIA were found on the composite surfaces (Fig. 6i and j). It is intriguing that diverse biofilms developed from different bacterial strains have distinct responses to photocatalysis for their removal. Before photocatalysis, biofilms developed from both *S. epidermidis* and *E. coli* O157: H7 completely covered the composite surfaces. The biofilms developed from *E. coli* O157: H7 had an even lower average thickness (33.8 ± 12.7 μm) compared with *S. epidermidis* (97.4 ± 68.3 μm). Hence it is not likely the abundance of biofilms on composite surfaces determines their resistance to removal. Different responses of EPS during photocatalysis could explain the discrepancy in biofilm eradication efficiency for diverse bacterial strains, and it highlights the importance of EPS destruction for biofilm removal. Future research will examine the structural and chemical properties of EPS of different biofilms to understand the mechanism of their resistance to photocatalytic oxidation.

3.5. Identification and quantification of reactive oxygen species (ROS) in photocatalysis for biofilm control

ROS generated during photocatalysis are believed to play important roles in biofilm inhibition and eradication, either by chemical reactions with biomolecules in biofilms (e.g., bacteria inactivation, EPS decomposition) or possibly biological interference with biofilms (e.g., quorum quenching) (Rumbaugh and Sauer, 2020). Herein, four kinds of possible ROS, i.e., ·OH, $O_2^{\cdot-}$, H_2O_2, and $^1O_2$ generated by carbon-doped g-C_3N_4/chitosan composites in photocatalysis were identified and quantified by specific radical probes (Zheng et al., 2019). The steady-state concentrations of $O_2^{\cdot-}$ and $^1O_2$ in photocatalysis were 5.49×10^{-12} and 2.86×10^{-13} M, respectively; and the accumulated concentration of H_2O_2 after 3 h of photocatalysis was 4.99 μM. The steady-state concentration of ·OH was too low to be detected ($<10^{-15}$ M). The concentrations of ROS generated by the photocatalyst-chitosan composites were comparable to those generated by g-C_3N_4 coupons in our previous study, i.e., $^1O_2$ (steady-state concentration of 3.32×10^{-13} M), $O_2^{\cdot-}$ (steady-state concentration of 4.44×10^{-13} M), and H_2O_2 (cumulative concentration of 1.69 μM after 2 h of photocatalysis) (Shen et al., 2019). The results indicate that the embedment of photocatalyst in chitosan did not impede ROS generation during photocatalysis. Many photocatalyst particles are likely to be on the composite surface and accessible to the photons in photocatalysis. Among three detectable ROS, H_2O_2 would exhibit a significant antibacterial effect only with a level of mM or even M. Therefore, in this study only $O_2^{\cdot-}$ and $^1O_2$ may play important roles in biofilm inhibition and eradication. To further pinpoint the key ROS, ROS quenching experiments were carried out. 10 mM FFA or 1 mM 4-hydroxy-TEMPO was used to quench $^1O_2$ or $O_2^{\cdot-}$, respectively, due to high reaction activity and selectivity between the ROS and the selected probes. The concentration of FFA or 4-hydroxy--TEMPO was optimized to minimize chemical toxicity to *S. epidermidis* bacterial cells (Fig. 7a, c, and e show many live bacteria in the dark, with or without the presence of scavengers). After photocatalysis, *S. epidermidis* bacterial cells adhered to the composite surfaces were completely inactivated without any scavenger or with 1 mM 4-hydroxy-TEMPO, however most of the *S. epidermidis* bacterial cells remained alive in the presence of 10 mM FFA (Fig. 7b, d, and f). Some CLSM images showed inevitable, hazy green background fluorescence

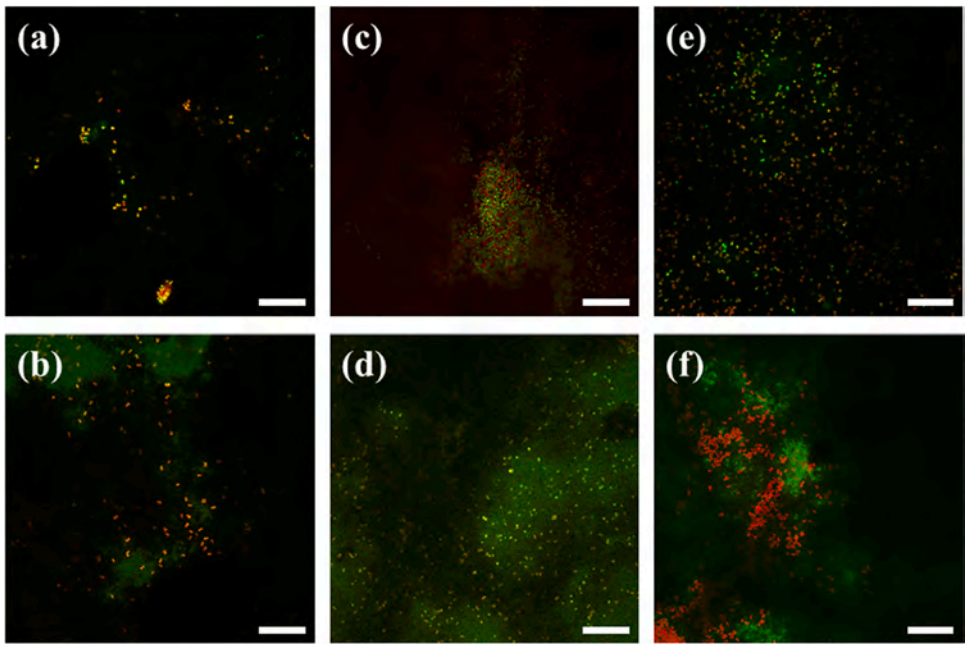

Fig. 7. ROS quenching experiments. (a) *S. epidermidis* bacteria in PBS, (c) *S. epidermidis* bacteria with 10 mM FFA, and (e) *S. epidermidis* bacteria with 1 mM 4-hydroxy-TEMPO on the photocatalyst-chitosan composite surfaces cultured in the dark for 1 h; (b) *S. epidermidis* bacteria in PBS, (d) *S. epidermidis* bacteria with 10 mM FFA, and (f) *S. epidermidis* bacteria with 1 mM 4-hydroxy-TEMPO on the photocatalyst-chitosan composite surfaces under the continuous irradiation of white LED light (7 W) for 1 h. Scale bars are 20 μm. The distance between the light source and the photocatalyst-chitosan composite surface was maintained at 15 cm. (For interpretation of the references to colour in this figure legend, the reader is referred to the web version of this article.)

(especially Fig. 7b, d, and f), since the photocatalyst-chitosan composites could be photoexcited by the laser in the characterization. Fortunately, the green background fluorescence is discernable from live staining of bacteria, which shows a unique round shape. The results provided a strong evidence that $^1O_2$ dominates bacterial inactivation. It is still unclear how $^1O_2$ with a short lifetime (ca. 2 μs in water) and a limited diffusion length can inactivate thick biofilms (Merkel and Kearns, 1972), and further investigation is needed. One plausible explanation is that the lifespan of $^1O_2$ significantly increased in the biofilms, due to a reduced collision frequency between $^1O_2$ and water (Maisch et al., 2007). In addition, the potential synergy of H_2O_2 with other ROS or oxidative stresses may turn bacteria susceptible to H_2O_2 as low as several μM, which may make H_2O_2 another key ROS determining antimicrobial performance of the photocatalyst-chitosan composites (Liu et al., 2020). Future research should further investigate the underlying antimicrobial mechanisms of photocatalysis for biofilm control.

3.6. Biofilm inhibition of photocatalyst-chitosan composites in urinary tract infections (UTI) patient urine

CAUTI-associated biofilms account for more than 30% of nosocomial infections, which results in billions of dollars in the medical cost in the U.S. each year (Stone, 2009). Compared with many other antimicrobial coatings or materials that can be potentially used for urinary catheters, including but not limited to Ag nanoparticles, enzymes, antibiotics, and polymeric modifications, the composites are robust and will provide long-lasting inactivation of biofilms when a suitable light source is introduced, because photocatalysis generates inexhaustible ROS continuously for inactivating biofilms (Singha et al., 2017). In addition, the composites that can inactivate biofilms developed from urine can be also broadly applied in fabricating self-cleaning surfaces of the sanitary wares (e.g., urinals and toilets). Here, we utilized UTI patient urine as both the growth medium and source of uropathogens to investigate the biofilm inhibition efficacy of the composites under visible light irradiation. UTI patient urine is comprised of complicated bacterial consortia growing in a specific but highly variable host-produced media, and it thus more closely mimics biofilm propagation on urinary catheters. The preliminary data (not included in this report) have shown that white LED light irradiation (flux of 3.11×10^2 μmol m^{-2} s^{-1} for photons with a shorter wavelength than 460 nm) was not able to inhibit biofilm development on the composite surfaces in the patient urine. As a consequence, blue LED light with an enhanced flux (flux of 1.07×10^3 μmol m^{-2} s^{-1} for photons with a shorter wavelength than 460 nm) was used for the experiments. The results suggested that mature and flourishing biofilms with an average thickness of 16.5 ± 24.9 μm and coverage of 35% occupied the composite surface after being incubated for 6 days in the UTI patient urine in the dark (Fig. 8a and c), whereas little to no biofilms were developed under blue LED light irradiation

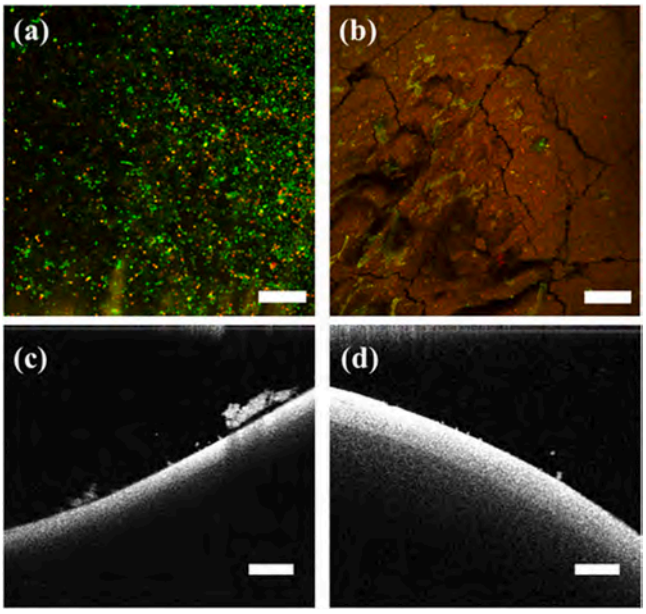

Fig. 8. Biofilm inhibition efficacy in the UTI patient urine. 2D-CLSM images of the composites in the UTI patient urine (a) in the dark and (b) under blue LED light irradiation (7 W) for 6 days; OCT images of the composites in the UTI patient urine (c) in the dark and (d) under blue LED light irradiation (7 W) for 6 days. Scale bars in 2D-CLSM and OCT images are 20 and 250 μm, respectively. The distance between the light source and the solution that submerged the photocatalyst-chitosan composites was maintained at 6 cm. (For interpretation of the references to colour in this figure legend, the reader is referred to the web version of this article.)

(Fig. 8b and d). The results demonstrated that the photocatalyst-chitosan composites exhibited excellent biofilm inhibition efficacy in UTI patient urine. In addition, the composites hold promise for medical applications requiring long-lasting antimicrobial performance by avoiding the issues such as exhaustiveness of antimicrobials and formation of conditioning films. Furthermore, the photoreactive antimicrobial urinary catheters could be achieved by the combination of photocatalysis and side glowing optical fibers, which can introduce light into the catheters uniformly (Lin et al., 2015).

4. Conclusion

Environmental pathogens in the form of biofilms cause serious health concerns and economic losses, such as drinking water contamination, nosocomial infections, and foodborne disease outbreaks. Due to their unique structural, physiochemical, and biological properties, biofilms hosting various environmental pathogens are much more persistent to conventional methods for pathogen control (e.g., antibiotics, oxidants, UV irradiation, heating, detergents, mechanical scrubbing and washing) than planktonic pathogens. Photocatalysis holds promise for inactivating and eradicating biofilms that contain environmental pathogens, because inexhaustible ROS are generated continuously in photocatalysis from activating oxygen gas, and they could inactivate bacteria and decompose EPS within biofilms rapidly and unselectively.

In this study, composites were developed from photocatalytic carbon-doped g-C_3N_4 and chitosan for pathogenic biofilm control. Carbon-doped g-C_3N_4 with a high photocatalytic activity continuously generates ROS and hence inactivates pathogens. The chitosan acts as a matrix for immobilizing the photocatalyst. The composite material is not only functional under ambient environment (by utilizing visible light including indoor light) but also shows enhanced processability for practical engineering applications. The photocatalytic composites can serve as active coatings for controlling biofilms in water and air purification, food packaging and processing, biomedical devices and equipment, sanitary wares, environmental surfaces, and many others. The photocatalytic composites were systematically characterized by SEM, ATR-FTIR, TG analysis, and BET surface area analysis to understand their physical, morphological, chemical, and thermal properties. All material characterizations demonstrate that the photocatalyst of carbon-doped g-C_3N_4 was well-distributed throughout the chitosan matrix. Next, broad-spectrum biofilm inhibition and eradication performance of the composites against a series of microorganisms under visible light irradiation were thoroughly investigated. The photocatalyst-chitosan composites completely inhibited biofilms developed from *S. epidermidis*, *P. aeruginosa* PAO1, and *E. coli* O157: H7 when exposed to continuous white LED light irradiation. In addition, photocatalysis was able to eradicate mature biofilms of *S. epidermidis* and *P. aeruginosa* PAO1 from the photocatalyst-chitosan composite surfaces. For mature biofilms developed from *E. coli* O157: H7, however, photocatalysis did not significantly remove the biomass even though a large portion of bacteria within biofilms were inactivated. Difficulty in removing *E. coli* O157: H7 biofilms was attributed to the resistance of EPS in biofilms to photocatalytic oxidation. The EPS of *S. epidermidis* and *P. aeruginosa* PAO1 biofilms were decomposed and removed during photocatalysis, whereas the EPS of *E. coli* O157: H7 biofilms were still found on the photocatalyst-chitosan composite surfaces after photocatalysis. However, increased light intensity and corresponding photoreactivity of the photocatalyst-chitosan composites successfully eradicated tough *E. coli* O157: H7 biofilms. Furthermore, ROS generated in photocatalysis were identified and quantified by radical probes, and $^1O_2$ was believed to play the key role in biofilm inhibition and eradication. Last but not least, the photocatalyst-chitosan composites also demonstrated excellent biofilm inhibition performance in UTI patient urine, which makes the material a promising candidate for inactivating biofilms developed from multiple bacterial species and developing antimicrobial urinary catheters or sanitary wares.

CRediT authorship contribution statement

Hongchen Shen: Conceptualization, Methodology, Formal analysis, Writing - original draft, Writing - review & editing. **David P. Durkin:** Investigation, Resources, Writing - original draft, Writing - review & editing, Funding acquisition. **Ashlee Aiello:** Investigation. **Tara Diba:** Investigation. **John Lafleur:** Investigation, Writing - original draft. **Jason M. Zara:** Investigation, Writing - original draft. **Yun Shen:** Conceptualization, Methodology, Resources, Writing - original draft, Writing - review & editing, Funding acquisition. **Danmeng Shuai:** Conceptualization, Methodology, Resources, Writing - original draft, Writing - review & editing, Supervision, Project administration, Funding acquisition.

Declaration of Competing Interest

The authors declare that they have no known competing financial interests or personal relationships that could have appeared to influence the work reported in this paper.

Acknowledgement

We acknowledge the United States Department of Agriculture-National Institute of Food and Agriculture Grant 2017-67021-26602, National Science Foundation Grant CBET-1929144, and Cross-Disciplinary Research Fund at The George Washington University for supporting our study. We also acknowledge the Air Force Office of Scientific Research (MIPR# F4FGA08354G001) and the United States Naval Academy for facilities support.

Appendix A. Supporting information

Supplementary data associated with this article can be found in the online version at doi:10.1016/j.jhazmat.2020.124890.

References

Becerril, R., Nerín, C., Silva, F., 2020. Encapsulation systems for antimicrobial food packaging components: an update. Molecules 25, 1134. https://doi.org/10.3390/molecules25051134.

Cangelosi, G.A., Freitag, N.E., Buckley, M., 2005. From outside to inside: environmental microorganisms as human pathogens. A Rep. Am. Acad. Microbiol. ⟨https://www.asmscience.org/content/report/colloquia/colloquia.14⟩.

Centers for Disease Control and Prevention (CDC), 2019. Surveillance for Foodborne Disease Outbreaks, United States, 2017, Annual Report. Atlanta, Georgia, U.S. Department of Health and Human Services, CDC.

Davies, D., 2003. Understanding biofilm resistance to antibacterial agents. Nat. Rev. Drug Discov. 2, 114–122. https://doi.org/10.1038/nrd1008.

Dohnalkova, A.C., Marshall, M.J., Arey, B.W., Williams, K.H., Buck, E.C., Fredrickson, J. K., 2011. Imaging hydrated microbial extracellular polymers: comparative analysis by electron microscopy. Appl. Environ. Microbiol. 77, 1254–1262. https://doi.org/10.1128/AEM.02001-10.

Evans, L.V., 2003. Biofilms: Recent Advances in Their Study and Control. CRC press.

Farid, M.U., Guo, J., An, A.K., 2018. Bacterial inactivation and in situ monitoring of biofilm development on graphene oxide membrane using optical coherence tomography. J. Membr. Sci. 564, 22–34. https://doi.org/10.1016/j.memsci.2018.06.061.

Flemming, H.C., Wingender, J., 2010. The biofilm matrix. Nat. Rev. Microbiol. 8, 623–633. https://doi.org/10.1038/nrmicro2415.

Flemming, H.C., Neu, T.R., Wozniak, D.J., 2007. The EPS matrix: the "house of biofilm cells". J. Bacteriol. 189.22, 7945–7947. https://doi.org/10.1128/JB.00858-07.

Gao, L., Pan, X., Zhang, D., Mu, S., Lee, D.J., Halik, U., 2015. Extracellular polymeric substances buffer against the biocidal effect of H_2O_2 on the bloom-forming cyanobacterium *Microcystis aeruginosa*. Water Res. 69, 51–58. https://doi.org/10.1016/j.watres.2014.10.060.

Huang, D., Wang, J., Ren, K., Ji, J., 2020. Functionalized biomaterials to combat biofilms. Biomater. Sci. 8, 4052–4066. https://doi.org/10.1039/D0BM00526F.

Johnson, J.R., Kuskowski, M.A., Wilt, T.J., 2006. Systematic review: antimicrobial urinary catheters to prevent catheter-associated urinary tract infection in hospitalized patients. Ann. Intern. Med. 144, 116–126. https://doi.org/10.7326/0003-4819-144-2-200601170-00009.

Koo, H., Allan, R.N., Howlin, R.P., Stoodley, P., Hall-Stoodley, L., 2017. Targeting microbial biofilms: current and prospective therapeutic strategies. Nat. Rev. Microbiol. 15, 740–755. https://doi.org/10.1038/nrmicro.2017.99.

Kumirska, J., Czerwicka, M., Kaczyński, Z., Bychowska, A., Brzozowski, K., Thöming, J., Stepnowski, P., 2010. Application of spectroscopic methods for structural analysis of chitin and chitosan. Mar. Drugs 8, 1567–1636. https://doi.org/10.3390/md8051567.

Lacroix-Gueu, P., Briandet, R., Lévêque-Fort, S., Bellon-Fontaine, M.N., Fontaine-Aupart, M.P., 2005. In situ measurements of viral particles diffusion inside mucoid biofilms. C. R. Biol. 328, 1065–1072. https://doi.org/10.1016/j.crvi.2005.09.010.

Liang, Q., Liu, X., Wang, J., Liu, Y., Liu, Z., Tang, L., Shao, B., Zhang, W., Gong, S., Cheng, M., He, Q., Feng, C., 2021. In-situ self-assembly construction of hollow tubular g-C_3N_4 isotype heterojunction for enhanced visible-light photocatalysis: experiments and theories. J. Hazard. Mater. 401, 123355 https://doi.org/10.1016/j.jhazmat.2020.123355.

Lin, B., Yuen, A.C.Y., Li, A., Zhang, Y., Chen, T.B.Y., Yu, B., Lee, E.W.M., Peng, S., Yang, W., Lu, H.D., Chan, Q.N., Yeoh, G.H., Wang, C.H., 2020. MXene/chitosan nanocoating for flexible polyurethane foam towards remarkable fire hazards reductions. J. Hazard. Mater. 381, 120952 https://doi.org/10.1016/j.jhazmat.2019.120952.

Lin, L., Wang, H., Luo, H., Xu, P., 2015. Enhanced photocatalysis using side-glowing optical fibers coated with Fe-doped TiO_2 nanocomposite thin films. J. Photochem. Photobiol. A Chem. 307.308, 88–98. https://doi.org/10.1016/j.jphotochem.2015.04.010.

Liu, H., Wu, Y.H., Ni, X.Y., Chen, Z., Peng, L., Huo, Z.Y., Wang, Q., Hu, H.Y., 2020. Construction and optimization mechanisms of carbon fiber-based flow-through electrode system (FES) with stackable multi-cathode units for water disinfection. J. Hazard. Mater. 399, 123065 https://doi.org/10.1016/j.jhazmat.2020.123065.

Liu, J., Dong, C., Deng, Y., Ji, J., Bao, S., Chen, C., Shen, B., Zhang, J., Xing, M., 2018. Molybdenum sulfide Co-catalytic Fenton reaction for rapid and efficient inactivation of *Escherichia coli*. Water Res. 145, 312–320. https://doi.org/10.1016/j.watres.2018.08.039.

López-Guerra, E.A., Shen, H., Solares, S.D., Shuai, D., 2019. Acquisition of time–frequency localized mechanical properties of biofilms and single cells with high spatial resolution. Nanoscale 11, 8918–8929. https://doi.org/10.1039/C8NR10287B.

Lu, W., Kiéné, L., Lévi, Y., 1999. Chlorine demand of biofilms in water distribution systems. Water Res. 33, 827–835. https://doi.org/10.1016/S0043-1354(98)00229-2.

Ma, R., Wang, G., Tian, Y., Wang, K., Zhang, J., Fang, J., 2015. Non-thermal plasma-activated water inactivation of food-borne pathogen on fresh produce. J. Hazard. Mater. 300, 643–651. https://doi.org/10.1016/j.jhazmat.2015.07.061.

Maisch, T., 2015. Resistance in antimicrobial photodynamic inactivation of bacteria. Photochem. Photobiol. Sci. 14, 1518–1526. https://doi.org/10.1039/C5PP00037H.

Maisch, T., Baier, J., Franz, B., Maier, M., Landthaler, M., Szeimies, R.M., Bäumler, W., 2007. The role of singlet oxygen and oxygen concentration in photodynamic inactivation of bacteria. Proc. Natl. Acad. Sci. U. S. A. 104, 7223–7228. https://doi.org/10.1073/pnas.0611328104.

Majeed, A., Sagar, F., Latif, A., Hassan, H., Iftikhar, A., Darouiche, R.O., Mohajer, M.A., 2019. Does antimicrobial coating and impregnation of urinary catheters prevent catheter-associated urinary tract infection? a review of clinical and preclinical studies. Expert Rev. Med. Devices 16, 809–820. https://doi.org/10.1080/17434440.2019.1661774.

Melton-Celsa, A.R., 2015. Shiga toxin (Stx) classification, structure, and function. In: Sperandio, V., Hovde, C.J. (Eds.), Enterohemorrhagic *Escherichia coli* and Other Shiga Toxin-Producing *E. coli*. John Wiley & Sons Ltd, pp. 37–53.

Merkel, P.B., Kearns, D.R., 1972. Radiationless decay of singlet molecular oxygen in solution. An experimental and theoretical study of electronic-to-vibrational energy transfer. J. Am. Chem. Soc. 94, 7244–7253. https://doi.org/10.1021/ja00776a003.

Midya, L., Patra, A.S., Banerjee, C., Panda, A.B., Pal, S., 2019. Novel nanocomposite derived from ZnO/CdS QDs embedded crosslinked chitosan: an efficient photocatalyst and effective antibacterial agent. J. Hazard. Mater. 369, 398–407. https://doi.org/10.1016/j.jhazmat.2019.02.022.

Nickel, J.C., Ruseska, I., Wright, J.B., Costerton, J.W., 1985. Tobramycin resistance of *Pseudomonas aeruginosa* cells growing as a biofilm on urinary catheter material. Antimicrob. Agents Chemother. 27, 619–624. https://doi.org/10.1128/AAC.27.4.619.

Okuda, T., Kokubu, E., Kawana, T., Saito, A., Okuda, K., Ishihara, K., 2012. Synergy in biofilm formation between *Fusobacterium nucleatum* and *Prevotella* species. Anaerobe 18, 110–116. https://doi.org/10.1016/j.anaerobe.2011.09.003.

Preston, M.J., Seed, P.C., Toder, D.S., Iglewski, B.H., Ohman, D.E., Gustin, J.K., Goldberg, J.B., Pier, G.B., 1997. Contribution of proteases and LasR to the virulence of *Pseudomonas aeruginosa* during corneal infections. Infect. Immun. 65.8, 3086–3090.

Rogers, K., 2010. Bacteria and Viruses. Britannica Educational Publishing.

Rumbaugh, K.P., Sauer, K., 2020. Biofilm dispersion. Nat. Rev. Microbiol. 18, 571–586. https://doi.org/10.1038/s41579-020-0385-0.

Schwering, M., Song, J., Louie, M., Turner, R.J., Ceri, H., 2013. Multi-species biofilms defined from drinking water microorganisms provide increased protection against chlorine disinfection. Biofouling 29.8, 917–928. https://doi.org/10.1080/08927014.2013.816298.

Shen, H., López-Guerra, E.A., Zhu, R., Diba, T., Zheng, Q., Solares, S.D., Zara, J.M., Shuai, D., Shen, Y., 2019. Visible-light-responsive photocatalyst of graphitic carbon nitride for pathogenic biofilm control. ACS Appl. Mater. Interfaces 11, 373–384. https://doi.org/10.1021/acsami.8b18543.

Singha, P., Locklin, J., Handa, H., 2017. A review of the recent advances in antimicrobial coatings for urinary catheters. Acta Biomater. 50, 20–40. https://doi.org/10.1016/j.actbio.2016.11.070.

Siqueira, V.M., Oliveira, H.M.B., Santos, C., Paterson, R.R.M., Gusmão, N.B., Lima, N., 2011. Filamentous fungi in drinking water, particularly in relation to biofilm formation. Int. J. Environ. Res. Public. Health 8, 456–469. https://doi.org/10.3390/ijerph8020456.

Srey, S., Jahid, I.K., Ha, S.D., 2013. Biofilm formation in food industries: a food safety concern. Food Control 31, 572–585. https://doi.org/10.1016/j.foodcont.2012.12.001.

Stone, P.W., 2009. Economic burden of healthcare-associated infections: an American perspective. Expert Rev. Pharm. Outcomes Res. 9, 417–422. https://doi.org/10.1586/erp.09.53.

Van Doremalen, N., Bushmaker, T., Morris, D.H., Holbrook, M.G., Gamble, A., Williamson, B.N., Tamin, A., Harcourt, J.L., Thornburg, N.J., Gerber, S.I., Lloyd-Smith, J.O., 2020. Aerosol and surface stability of SARS-CoV-2 as compared with SARS-CoV-1. N. Engl. J. Med. 382.16, 1564–1567. https://doi.org/10.1056/NEJMc2004973.

Vuong, C., Otto, M., 2002. *Staphylococcus epidermidis* infections. Microbes Infect. 4, 481–489. https://doi.org/10.1016/S1286-4579(02)01563-0.

World Health Organization, 2017. Progress on Drinking Water, Sanitation and Hygiene: 2017 update and SDG baselines." ⟨https://www.who.int/water_sanitation_health/publications/jmp-2017/en/⟩.

Yang, K., Li, L., Wang, Y., Xue, S., Han, Y., Liu, J., 2019. Airborne bacteria in a wastewater treatment plant: emission characterization, source analysis and health risk assessment. Water Res. 149, 596–606. https://doi.org/10.1016/j.watres.2018.11.027.

Yang, X., Ou, C., Yang, H., Liu, L., Song, T., Kang, M., Lin, H., Hang, J., 2020. Transmission of pathogen-laden expiratory droplets in a coach bus. J. Hazard. Mater. 397, 122609 https://doi.org/10.1016/j.jhazmat.2020.122609.

Yuan, W., Zhang, Y., Riaz, L., Yang, Q., Du, B., Wang, R., 2021. Multiple antibiotic resistance and DNA methylation in enterobacteriaceae isolates from different environments. J. Hazard. Mater. 402, 123822 https://doi.org/10.1016/j.jhazmat.2020.123822.

Zheng, Q., Durkin, D.P., Elenewski, J.E., Sun, Y., Banek, N.A., Hua, L., Chen, H., Wagner, M.J., Zhang, W., Shuai, D., 2016. Visible-light-responsive graphitic carbon nitride: rational design and photocatalytic applications for water treatment. Environ. Sci. Technol. 50, 12938–12948. https://doi.org/10.1021/acs.est.6b02579.

Zheng, Q., Shen, H., Shuai, D., 2017. Emerging investigators series: advances and challenges of graphitic carbon nitride as a visible-light-responsive photocatalyst for sustainable water purification. Environ. Sci. Water Res. Technol. 3.6, 982–1001. https://doi.org/10.1039/C7EW00159B.

Zheng, Q., Xu, E., Park, E., Chen, H., Shuai, D., 2019. Looking at the overlooked hole oxidation: photocatalytic transformation of organic contaminants on graphitic carbon nitride under visible light irradiation. Appl. Catal. B Environ. 240, 262–269. https://doi.org/10.1016/j.apcatb.2018.09.012.

Zheng, Q., Aiello, A., Choi, Y.S., Tarr, K., Shen, H., Durkin, D.P., Shuai, D., 2020. 3D printed photoreactor with immobilized graphitic carbon nitride: a sustainable platform for solar water purification. J. Hazard. Mater. 399, 123097 https://doi.org/10.1016/j.jhazmat.2020.123097.